Published in final edited form as:
Neuroscience. 2008 October 15; 156(3): 498–514. doi:10.1016/j.neuroscience.2008.08.013.

ROBUST AXONAL GROWTH AND A BLUNTED MACROPHAGE RESPONSE ARE ASSOCIATED WITH IMPAIRED FUNCTIONAL RECOVERY AFTER SPINAL CORD INJURY IN THE MRL/MpJ MOUSE

S. K. KOSTYK[a,b,e], **P. G. POPOVICH**[b,c,e], **B. T. STOKES**[d], **P. WEI**[b,e], and **L. B. JAKEMAN**[b,d,e,*]

a *Department of Neurology, The Ohio State University Medical Center, Columbus, OH 43210, USA*

b *Department of Neuroscience, The Ohio State University Medical Center, Columbus, OH 43210, USA*

c *Department of Molecular Virology, Immunology and Medical Genetics, The Ohio State University Medical Center, Columbus, OH 43210, USA*

d *Department of Physiology and Cell Biology, The Ohio State University Medical Center, 304 Hamilton Hall, 1645 Neil Avenue, Columbus, OH 43210, USA*

e *Center for Brain and Spinal Cord Repair, The Ohio State University Medical Center, Columbus, OH 43210, USA*

Abstract

Spinal cord injury (SCI) in mammals leads to a robust inflammatory response followed by the formation of a glial and connective tissue scar that comprises a barrier to axonal regeneration. The inbred MRL/MpJ mouse strain exhibits reduced inflammation after peripheral injury and shows true regeneration without tissue scar formation following an ear punch wound. We hypothesized that following SCI, the unique genetic wound healing traits of this strain would result in reduced glial and connective tissue scar formation, increased axonal growth, and improved functional recovery. Adult MRL/MpJ and C57BL/6J mice were subjected to a mid-thoracic spinal contusion and the distribution of axon profiles and selected cellular and extracellular matrix components was compared at 1, 2, 4 and 6 weeks post-injury. Recovery of hind-limb locomotor function was assessed over the same time period. The MRL/MpJ mice exhibited robust axon growth within the lesion, beginning at 4 weeks post-injury. This growth was accompanied by reduced macrophage staining at 1, 2, 4 and 6 weeks post-injury, decreased chondroitin sulfate proteoglycan staining at 1–2 weeks and increased laminin staining throughout the lesion at 2–6 weeks post-injury. Paradoxically, the extent of locomotor recovery was impaired in the MRL/MpJ mice. Close examination of the chronic lesion site revealed evidence of ongoing degeneration both within and surrounding the lesion site. Thus, the regenerative genetic wound healing traits of the MRL/MpJ mice contribute to the evolution of a lesion environment that supports enhanced axon growth after SCI. However, this response occurs at the expense of meaningful functional recovery.

Keywords

regeneration; degeneration; contusion; inflammation; astrocyte; glial scar

*Correspondence to: L. Jakeman, Department of Physiology and Cell Biology, 304 Hamilton Hall, 1645 Neil Avenue, Columbus, OH 43210, USA. Tel: +1-614-688-4424; fax: +1-614-292-4888. E-mail address: jakeman.1@osu.edu (L. Jakeman).

Tissue regenerative capacity varies across phylogeny, with complete epimorphic regeneration in planarians (Reddien and Sanchez Alvarado, 2004) and axolotls (Chernoff et al., 2003), and the loss of this capacity during metamorphosis in the tadpole (Beattie et al., 1990). Most adult mammals show no true regenerative ability, with the exception of the pinna of the rabbit ear and the wings of bats (Church and Warren, 1968; Goss and Grimes, 1975). In other tissues, injury initiates a cellular response including activation and recruitment of circulating inflammatory cells. These interact with resident cells to enhance connective tissue deposition, scar tissue formation and wound contraction to restore tissue and vascular integrity at the injury site (Werner et al., 2007).

Injury to the mammalian CNS is characterized by similar events, leading to glial activation and connective tissue scar formation at the site of injury allowing little or no axonal regeneration. Within hours to days after trauma, activated neutrophils, macrophages, mesenchymal cells and leukocytes are recruited to the site of injury (Zhang et al., 1996; Popovich et al., 1997; Sroga et al., 2003). Astrocytes vacate the lesion center, proliferate, undergo hypertrophy and accumulate at the edges of the injury site (Fitch et al., 1999; Fitch and Silver, 2008). Together with other glial cell populations, they up-regulate their expression of growth inhibitory molecules, including chondroitin sulfate proteoglycans (CSPGs), which correlate with regions of abortive axonal growth (Davies et al., 1997, 1999). The scar surrounding a CNS injury site thus creates a physical and chemical barrier that impedes successful regeneration of severed and surviving axons.

There are some conditions where true regeneration is observed in the mammalian CNS suggesting that the capacity to achieve functional connectivity may exist. For example, functional regeneration is observed after spinal cord transection in opossums and rats during early gestational development (Wang et al., 1996; Fry et al., 2003; Lane et al., 2007). In addition, long distance axon regeneration within the spinal cord is observed after a crush injury of the adult rat filum terminale (Kwiecien and Avram, 2008). In the exceptional cases in both the periphery and CNS, successful regeneration is supported by underlying cellular events, including limited local inflammation, the formation of a blastema or ependymal proliferation at the wound edge, and the absence of chronic glial scar or fibrotic scar tissue formation at the site of injury (Chernoff et al., 2002; Ferretti et al., 2003; Slack et al., 2004; Lane et al., 2007).

Recent studies have identified two genetically inbred strains of mice that display scarless, epimorphic healing of somatic tissues. Notably, the MRL/MpJ and its ancestral strain, LG/J, both exhibit a rapid regenerative healing response, with complete wound closure by 4 weeks after a standard 2-mm ear punch injury. Compared with several other strains, the ear wounds of these mice develop increased edema, angiogenesis, fibroblast (Fb) migration, and decreased scarring and fibrosis at the wound site. True regeneration is evident with formation of new cartilage, vessels, hair follicles and skin from a blastema-like structure formed at the edges of the injury (Clark et al., 1998; Li et al., 2001a). These mice also exhibit scarless healing after a cryogenic injury to the heart or corneal alkali burn damage (Leferovich et al., 2001; Ueno et al., 2005), although fibrosis is evident with larger wounds (Beare et al., 2006; Colwell et al., 2006). Measurements of protein and mRNA levels at the site of the healing wounds have revealed a pattern consistent with a reduced inflammatory response, earlier expression of tissue repair genes and reduced deposition of extracellular collagens in this strain (McBrearty et al., 1998; Li et al., 2001b). Because inflammation and extracellular matrix deposition are also key elements of the scar formation process that impedes CNS axonal regeneration, we tested the hypothesis that the unique regenerative traits in the MRL/MpJ mouse strain would result in the formation of a cellular and extracellular environment that would support axonal regeneration and tissue repair and improve functional recovery after spinal cord injury (SCI). We compared the extent of axon growth, the distribution of astrocytes and their processes,

patterns of extracellular CSPGs, laminin and fibronectin and general ultrastructural features at the lesion site after spinal contusion injury in MRL/MpJ mice with the well-studied C57BL/6 mice. The results demonstrate the existence of an intriguing dichotomy in the cellular and tissue dynamics of the MRL/MpJ mouse strain. A marked reduction in local inflammation was associated with the formation of a permissive environment for axonal growth into the lesion at later time points. However, the MRL/MpJ mice also showed impaired functional recovery, which may be a consequence of pronounced lesion constriction and the presence of an increasingly loosely structured cellular terrain at the site of injury. These results demonstrate that genetically-encoded wound-healing traits in the MRL/MpJ mouse help reduce the growth-inhibitory nature of the glial and fibrotic scar at the lesion site; however, these events can prove detrimental to the restoration of tissue integrity and occur at the expense of functional recovery.

EXPERIMENTAL PROCEDURES

Animals, surgery, and care

A total of 74 adult female C57BL/6J (*N*=35) and MRL/MpJ mice (*N*=39) were used in these experiments (The Jackson Laboratory, Bar Harbor, ME, USA). All procedures were carried out in accordance with the Ohio State University Institutional Animal Care and Use Committee and the National Research Council Guide for the Use and Care of Laboratory Animals. Spinal cord contusion injury was performed using an electromagnetic device described in detail elsewhere (Jakeman et al., 2000; Ma et al., 2001). Mice were anesthetized with ketamine (80 mg/kg) and xylazine (10 mg/kg; i.p.), and a dorsal laminectomy (1.5 mm×1.7 mm) was prepared at the ninth thoracic vertebral level. The mice were injured by a rapid displacement of an impounder (1.35 mm tip diameter) 0.5 mm over an ~23 ms period (moderate severity). Subjects were age-matched to ensure similar developmental cellular maturity. Because MRL/MpJ mice were initially bred for their large size, the groups differed in total starting weight (MRL/MpJ 30.6±0.5 g and C57BL/6J=17.3±0.2 g; 10 weeks of age at time of injury). However, there were no differences in mid-thoracic spinal cord diameters of control animals or in the diameter of the spinal cords across strains at 1.5 mm rostral or caudal to the lesion center. There were no differences in peak displacement, peak force, or impulse/momentum measured at the time of spinal cord impact. Post-operative care included daily inspection, manual bladder expression, s.c. administration of 0.9% saline during the first 5 days post-injury (dpi), antibiotic (Gentacin, gentamicin sulfate 100; Vedco, Inc., St. Joseph, MO, USA; 5 mg/kg) and acidified drinking water (pH <4.0) to discourage bladder infection. Mortality across both strains was less than 5% over the duration of the study. In the course of the experiments, five MRL/MpJ mice exhibited some swelling or bite-marks on a hind limb and were treated for 1–5 days by wrapping the affected limb. Behavioral testing was not performed during treatment.

Histological analysis

Pilot studies were performed to obtain specimens at 2, 7, 14, and 28 dpi (*n*=2–3 per strain per time point). After a review of preliminary staining patterns and functional outcomes, the time course was extended. Additional specimens were obtained at 7, 14, 28 and 42 dpi (*n*=6/strain per time point) for determination of lesion size and quantitative analysis of cellular and extracellular composition. At the indicated dpi, the mice received an overdose of ketamine/xylazine anesthesia and were perfused transcardially with phosphate-buffered saline (PBS) followed by 4% paraformaldehyde in PBS (pH 7.4). The spinal cords were post-fixed for 2 h, and transferred to 0.2 M sodium phosphate buffer overnight at 4 °C. Tissues from a 6-mm block centered on the site of impact were cryoprotected in 30% sucrose and sectioned in 10 adjacent sets at 10-μm thick. Every slide contained specimens from both strains; all slides for each stain were processed concurrently using the same working solutions. A researcher who was blind to strain and time post-injury performed analyses.

For traditional analysis of white matter sparing at the lesion epicenter, one series of transverse sections was stained with 0.1% Luxol Fast Blue (LFB) to identify phospholipids. The lesion epicenter was defined as the tissue section with the smallest cross-sectional area of normal LFB staining in the peripheral rim (Behrmann et al., 1992). The total cross-sectional area (TCSA) of the spinal cord and the peripheral boundary of residual LFB staining (spared white matter; SWM) were measured on digitized images from the epicenter and 200, 400, 600, 800, 1000 and 1500 μm rostral and caudal to this section using a computer-assisted image analysis program (MCID; Imaging Research Inc., Ontario, Canada) and manually outlining each image while viewing the tissue sections under the light microscope (Zeiss Axiophot with 20× objective). SWM was expressed as mm^2 and also calculated as a percentage (%) of the TCSA of the cord at each level (Bresnahan et al., 1987; Basso et al., 1996). Lesion length was determined to the nearest 100 μm by examining the LFB stained sections rostrally and caudally from the epicenter (Ma et al., 2001).

Immunocytochemical staining and analysis

Rabbit polyclonal antisera were used to detect markers present in astrocytes (glial fibrillary acidic protein, GFAP; DAKO Corporation, Carpinteria, CA, USA), and axons (200 kDa neurofilament (NF) protein, NF, Chemicon, Temecula, CA, USA). A monoclonal rat anti-mouse CD11b antibody was used to identify surface receptors on microglia and macrophages (clone Mac-1; Serotec MCA74; AbD Serotec Inc., Raleigh, NC, USA). Extracellular matrix proteins were identified with rabbit polyclonal antisera specific for laminin (anti-EHS laminin; Sigma-Aldrich, St. Louis, MO, USA), and fibronectin (anti-human fibronectin, Sigma-Aldrich) or monoclonal (mouse IgM) antibodies raised against chondroitin sulfate preparations that recognizes the glycosaminoglycan (GAG) residues present on some CSPG molecules (CS56, Sigma-Aldrich). Sections were pretreated with 0.1% Triton X-100 either with 4% bovine serum albumin in PBS, 2–10% normal goat serum in PBS, or 0.0025% trypsin in 0.1% CaCl2 for 5 min at 37 °C followed by 2% BSA in PBS (fibronectin only). Primary antibodies were applied at 4 °C overnight and secondary biotinylated antibodies (Vector Laboratories, Burlingame, CA, USA, or Jackson Immunoresearch Laboratories, West Grove, PA, USA) were applied at 1:400 for 2 h at room temperature. For CS56, the primary and secondary antibodies were pooled and mixed with 0.1% normal mouse serum prior to incubation on slides. Detection was performed using avidin–biotin complex (Vector ABC Elite) with 0.06% H_2O_2 as a catalyst and diaminobenzidine or SG as chromogens (Vector Laboratories). All sections were viewed using a Zeiss Axiophot. Regions for analysis were digitized with a 24-bit CCD color camera (SONY 970) and saved using the MCID software. Target areas and proportional area (PA) measures of positively stained profiles and regions were obtained across time and strains. PA was computed as the area of positive staining (Target area) divided by the reference area as described previously (Popovich et al., 1997; Sroga et al., 2003; Ma et al., 2004).

Behavioral recovery

Locomotor function was initially assessed using the Basso Beattie Bresnahan (BBB) rating scale (Basso et al., 1995; Ma et al., 2001). Each mouse was observed for 4 min by a team of two investigators who assigned a score value to each hind limb. Since the completion of theses experiments, a locomotor rating scale, termed the Basso mouse scale (BMS) has been developed specifically for use with spinal cord injured mice (Basso et al., 2006). Completed BBB data sheets for each of the testing sessions were reviewed and rescored according to objective definitions of the BMS rating scale and the data plotted and analyzed for comparison with current standards.

Fine structure

To further evaluate the composition of the chronic injury site, three injured specimens from each strain were obtained at 42 dpi, perfused with 4% paraformaldehyde in PBS and post-fixed overnight in 2% glutaraldehyde in 10% sucrose. Blocks of 1 mm^2 from the lesion epicenter were incubated for 4 h in OsO_4, dehydrated and embedded in Spurrs resin. Sections were cut at 1 μm thickness and stained with 1% Toluidine Blue. Representative blocks were sectioned further with an ultramicrotome; thin sections were stained with uranyl acetate or left unstained and examined at the ultrastructural level using an FEI Tecnai G2 Bio TWIN transmission electron microscope.

Statistical analysis

Two-way analysis of variance (ANOVA) with repeated measures was used to compare cross-sectional area measures, PA measures and BBB or BMS scores across strains with dpi or distance from epicenter as the second independent variable (Scheff et al., 2002). Strain differences were compared at each time point or distance from the epicenter using Bonferroni corrected post hoc *t*-tests. All graphs illustrate group means ± standard error of the mean (S.E.M.), and data were analyzed and plotted using Prism 4.03 for Windows (GraphPad Software, Inc., La Jolla, CA, USA, ©2005).

Images

Images were collected in .TIF format using the image capture features of the MCID System, and figure plates were assembled using Photoshop CS (Adobe, Inc.). Brightness and contrast were adjusted if required, and some color images were converted to grayscale for production of plates. No enhancement of images was performed prior to any quantitative measurements.

RESULTS

Axonal growth is enhanced within the MRL/MpJ lesion site

Spinal cord contusion results in a primary hemorrhage and loss of neurons and glial cells at the center of the site of impact. This leaves a rim of spared tissue corresponding to the location of residual ascending and descending white matter tracts (Basso et al., 1996; Ma et al., 2001). To investigate the influence of the MRL/MpJ genetic background on axonal growth after SCI, sections through the lesion at 2, 7, 14, 28 and 42 dpi were stained with anti-NF antibodies. From 2–14 dpi, NF staining was similar in both strains as described previously for C57BL/6J (Ma et al., 2004). At 2 dpi, the lesion site was occupied by NF-stained debris that was cleared by 7 dpi. At 7 and 14 dpi, there were very few axon profiles and minimal NF staining in the lesion site and no differences in staining pattern between the two strains. At all time points, NF staining was present in axon profiles cut in their transverse orientation throughout the surrounding white matter. Beginning at 28 dpi in the MRL/MpJ mice, there was a marked increase in axonal profile density in the center of the lesion (Fig. 1A–D). The axons were randomly oriented and were distributed throughout the entire lesion. Using a density threshold to quantify the area occupied by axons, both the total NF-stained area and the proportion of the central region occupied by axons (Fig. 1G) were increased by as much as threefold at both 28 and 42 dpi in the MRL/MpJ mice. On average, the stained axons alone occupied 10–15% of the total area in the lesion center in MRL/MpJ mice, compared with less than 3–5% as seen previously in C57BL/6J mice. Tract tracing studies were not performed, but a subset of the axons within the MRL/MpJ lesion exhibited CGRP-immunoreactivity, indicating that at least some of the fibers were derived from peptidergic primary afferents (Fig. 1H). In contrast, axons stained with 5-HT antibodies accumulated and terminated at the rostral and lateral edges of the lesion in both strains, and did not extend to the lesion center at either 28 or 42 dpi.

Recovery of hind limb locomotion

To determine if the increased axonal growth in the MRL/MpJ mice would support improved functional recovery, the mice were tested using the BBB/BMS open field locomotor test and compared with C57BL/6J mice. All mice scored normally (BMS=9) before injury. They all showed complete paralysis beginning 1 dpi, followed by partial recovery over the next 3–4 weeks (Fig. 2). Despite the increased axonal density in the lesion of MRL/MpJ mice, the locomotor performance of the MRL/MpJ mice was consistently worse than that of the C56BL/6J mice ($P<0.0001$). The average score of the C57BL6/J mice at 28–42 dpi was 5.4, indicating frequent to consistent stepping, while the average score of the MRL/MpJ mice over the same time points was 3.0–3.5, corresponding to none or occasional stepping.

Upon initial examination of the histological specimens, it became clear that there were tissue organizational differences within the lesion region that were increasing evident at later time points. To better understand how increased axonal growth could be associated with impaired functional recovery, we undertook a detailed comparison of the lesion pathology in the two strains using immunocytochemistry and plastic sections.

Lesion size and tissue sparing

In mouse and rat contusion SCI models, the extent of locomotor recovery correlates closely with the cross-sectional area of residual myelinated fiber tracts present in the peripheral rim of transverse sections taken through the lesion epicenter (Noble and Wrathall, 1989; Behrmann et al., 1992; Ma et al., 2001). In both strains, the primary features of the epicenter included a central region of tissue damage surrounded by a rim of SWM (Fig. 3A, B). The center of the lesion was filled with cells and matrix materials that stained lightly with the LFB stain. The TCSA and SWM area was measured using classical methods in serial frozen transverse sections obtained at each time point (Fig. 3C, D). Both strains had significant shrinkage of the spinal cord epicenter TCSA over time, but the MRL/MpJ specimens underwent a greater contracture as early as 7 dpi (Fig. 2E). Expression of the SWM area as a proportion of the TSCA was also used to correct for differential shrinkage of the spinal cord across the strains, but no significant differences in the percentage of SWM were found (two-way ANOVA; effect of dpi: $P<0.001$; strain $P=0.325$). The demonstration of similar WMS areas suggested that the behavioral deficits in MRL/MpJ mice might be due to other ongoing pathology within and surrounding at the lesion site.

Macrophage invasion and demarcation of the lesion epicenter

The MRL/MpJ mice exhibit a reduced local inflammatory response after an ear punch or corneal wound (McBrearty et al., 1998; Ueno et al., 2005). To determine if inflammation is also diminished after SCI, the Mac-1 antibody, which recognizes the CD11b receptor (CR3) on mouse macrophages, monocytes and microglia, was used to compare the time course of the inflammatory response in the spinal cord after contusion injury. The intensity and distribution of staining was first compared and measured at low magnification (Fig. 4A–E). At 7 dpi, the differences were subtle. The C57BL/6J epicenter contained dense Mac-1 staining, which filled the lesion center and much of the surrounding tissue rim (Fig. 4A). The epicenter of the MRL/MpJ lesion site at 7 dpi was similar in appearance, it also contained dense Mac-1 positive staining, but the occupied regions were smaller (Fig. 4B). By 14 dpi, however, the C57BL/6J injury site was completely occupied by large clusters of tightly packed rounded cellular profiles (Fig. 4C, c′), which remained through 42 dpi, increasing in staining intensity over time (Fig. 4E–G). Indeed a distinct border between the central core region and the peripheral white matter was demarcated in this strain from 14 dpi onward, with the largest phagocytic profiles restricted to the center and reactive microglia and occasional phagocytic profiles found throughout the rim (Fig. 4C, E–G). In contrast, CD11b staining in the center of the MRL/MpJ specimens was markedly reduced by 14 dpi, although activated microglial-like profiles were still evident along

the lesion border (Fig. 4D). Staining in the MRL/MpJ mice continued to decrease over time. At 28 and 42 dpi, the Mac-1 staining in the center and the rim of the spinal cord was barely detectable at low or high power, in comparison with the dense staining found in the C57BL/6J lesion core and surrounding rim (Fig. 4E, H).

Measurements of the total area of CD11b (Mac-1) immunoreactivity from the lesion epicenter sections underscored the qualitative differences in the local inflammatory response. Two-way ANOVA of total stain (target) area and % TCSA occupied by Mac-1 immunoreactivity revealed a strong effect of strain ($P<0.0001$) and dpi ($P<0.0001$), and an interaction effect ($P=0.008$) (Fig. 4I, J). The C57BL/6J mice had greater CD11b expression at all time points, and the interaction reflected a monophasic decrease in staining in MRL/MpJ mice in contrast with an apparent secondary increase in the proportion of Mac-1 staining in C57BL/6J mice corresponding to a late increase in leukocyte and possibly T-cell recruitment and CD11b expression as described previously (Sroga et al., 2003; Ma et al., 2004; Kigerl et al., 2006).

Astrocyte distribution and gliosis

Differences in Mac-1 staining along the lesion border suggested that the residual rim of tissue evolves differently in the two strains despite the similar PA measures of traditional LFB staining. Specifically, the peripheral rim of spared tissue is largely associated with hypertrophic glial cells and processes and the formation of a glial barrier to axonal regeneration. To test the hypothesis that the astrocyte response was delayed, reduced, or prevented in the MRL/MpJ mice, we examined the distribution of staining with the glial filament marker, GFAP, over time. Surprisingly, the gross characteristics of the astrocytic response viewed at low power were similar in both strains. GFAP staining was associated with debris at 2 dpi and by 7 dpi, and astrocytes were absent from the center of the lesion of both strains at these times. By 14 dpi, both strains had a large astrocyte-free central region and a strongly reactive region of astrogliosis in the surrounding white matter (Fig. 5A, B). The staining intensity was similar and there were no significant differences in the cross-sectional area or percentage of the cross-sectional area occupied by GFAP immunoreactivity over time (dpi $P<0.001$; strain $P>0.05$; interaction $P>0.05$). However, inspection of the staining pattern and morphological features in the rim of the specimens at higher power revealed qualitative differences at 28 and 42 dpi (Fig. 5C, D). A homogenous pattern of GFAP staining dominated by radial-oriented glial profiles was predominant within the white matter rim of the C57BL/6J specimens, with a well-demarcated border of aligned GFAP+ processes at the lesion edge (arrows Fig. 5c″). In contrast, at these more chronic time points, the astrocyte border in the MRL/MpJ mice was not well defined, the processes were less tightly intertwined and the staining pattern of the residual white matter regions was irregular and contained large regions devoid of GFAP staining (Fig. 5d′,d″; asterisks). Thus, the GFAP staining suggested a loss of glial scar integrity at the later time points in the residual white matter rim compared with the well-studied C57BL/6J mice.

Composition of the peripheral rim

To determine if the differences in astrocyte distribution corresponded with differences in cellular organization within the rim, 1-μm sections through the epicenter in 42 dpi specimens were stained with Toluidine Blue (Fig. 5E, F). In the C57BL/6J mice, the peripheral rim was densely packed with glial processes, some myelinated axons, degenerating myelin, occasional myelin ghosts and a few enlarged blood vessels. Notably, there was very little extracellular space in the residual white matter at this time point. In contrast, the white matter rim of the MRL/MpJ mice contained large numbers of enlarged degenerating axon profiles and myelin debris, greater extracellular space between the profiles and a generally disorganized tissue appearance. Therefore, although the traditional LFB measures and GFAP staining revealed no quantitative differences in the amount of gross residual white matter area between the two

strains, closer examination of the tissues showed that the cellular integrity of the residual rim of tissue was worse in the MRL/MpJ mice than the C57BL/6J by 42 dpi.

Cellular composition of the lesion center

Once identified, it became clear that the differences in the fine structure and organization of the lesion site at these later time points were not restricted to the residual white matter. The chronic 42 dpi C57BL/6J sections showed a well-demarcated central region of tightly packed, lipid-filled macrophage clusters (MC), that corresponded to the dense Mac-1 stained profiles seen earlier, which were clearly separated from the spared tissue by a border of tightly packed glial processes (GB; Fig. 6A, C, E). Notably, the lesion center contained a minimum of extracellular space between the macrophage profiles. The cells found between the MCs contained dark nuclei and cytoplasm and had leading processes resembling those of Fb (Fig. 6G). In contrast, as predicted by the immunocytochemical staining patterns, the MRL/MpJ specimens exhibited a much more irregular and heterogeneous pattern of cells and processes at the edges of the lesion and throughout the section, making a precise border difficult to discern (Fig. 6B, D). Despite the smaller cross-sectional area and contraction of the MRL/MpJ specimens, the center of these lesions contained profiles of degenerating axons, myelin ghosts and debris, and increased extracellular space with loosely organized cells and collagen fibrils (Fig. 6D, F, H). One feature seen in the MRL/MpJ mice that was absent from the C57BL/6J specimens were occasional clusters of small cells with darkly stained cytoplasm (Fig. 6D, dcc) that could be found at the periphery or in the center of the lesions. While the source of these cells is not known, they suggest a proliferative and relatively undifferentiated cell phenotype.

Distribution of extracellular matrix substrates

Previous descriptions of scar tissue after injury in C57BL/6 mouse spinal cord have shown a predominance of fibronectin deposition over time (Zhang et al., 1996; Jakeman et al., 2000; Sroga et al., 2003; Ma et al., 2004; Kigerl et al., 2006). Given the differences in inflammatory cell distribution and staining intensity, it was surprising that the distribution and density of fibronectin immunoreactivity were similar to published reports on C57BL/6 mice with no obvious differences between these strains from 7 to 28 dpi. At 42 dpi, however, there were differences in the staining pattern between the strains. Specifically, the fibronectin staining was much denser in the C57BL/6J mice and clearly surrounded the MCs that were present throughout the lesion center (Fig. 7A, C). In contrast, fibronectin staining in MRL/MpJ lesions was lighter, wispy in appearance and heterogeneously distributed (Fig. 8B, D). Some of the staining was diffuse and extracellular in nature, while some small profiles resembled the surface of cells lined with fibronectin. The fibrotic tissue scar characteristic of the mouse contusion injury core showed the greatest differences at the most chronic time point.

Both strains also exhibited similar features of laminin staining at 7 and 14 dpi, with laminin staining initially high and then restricted to blood vessels and along the border demarcated by GFAP immunoreactivity by 14 days. However, these patterns diverged markedly in the 28 and 42-day tissues. In C57BL/6J mice, the laminin immunoreactivity remained restricted to the glial limiting border and surrounding blood vessels at both 4 and 6 weeks post-injury (Fig. 8E, G). In contrast, the distribution of laminin immunoreactivity continued to expand in the MRL/MpJ mice. Regions of enhanced reactivity were evident in the peripheral white matter rim and along blood vessels, while extravascular laminin reactivity in the center of the lesion increased so that the entire lesion site was highly laminin-reactive at 28 and 42 dpi (Fig. 7F, H). In summary, these matrix-staining patterns reveal a reduced fibronectin and greater laminin prominence in the MRL/MpJ strain.

CSPGs and their GAG side chains are upregulated after SCI and represent a major inhibitor of growth cone extension in the glial scar (Fitch and Silver, 2008). To determine if the enhanced

axon growth in the MRL/MpJ mice could be attributed to a difference in the molecular composition of the glial scar, sections from specimens taken at 7 and 14 dpi, when CSPG expression is maximal in the C57BL/6J mice (Ma et al., 2004), were stained with the CS56 monoclonal antibody, which recognizes the GAG chains on some CSPGs. In both strains of mice, CSPG-GAGs were found within the dorsal and ventral roots and at the dorsal root entry zone at the lesion site (Fig. 8). In the C57BL/6J mice, CSPGs were also upregulated at the edges of the lesion center at 7 and 14 dpi, corresponding to the distribution of astrocytes and glial processes at the lesion border (Fig. 8A, C, D). As found previously, very little staining was found within the center of the lesion in these mice. In striking contrast, sections through the lesion site of the MRL/MpJ mice stained under identical conditions showed little to no reactivity, either in the lesion center or the peripheral rim of tissue (Fig. 8B). Thus, differences in the composition of the extracellular matrix in the MRL/MpJ mice include an apparent reduction in the expression of the inhibitory CSPG GAG chains along the lesion border.

DISCUSSION

The comparison of SCI lesion pathology in MRL/MpJ and C57BL/6J emphasizes the great potential of the mammalian CNS to express a wide range of cellular and molecular responses to trauma. While both strains initiated the recruitment of inflammatory cells and glial activation, these events were greater as early as 7–14 dpi in the C57BL/6J mice, as shown by quantitative measures of CD11b expression. The corresponding reduced CSPG-GAG expression in MRL/MpJ mice during this time frame suggests a reduced astrocyte activation and a lower inhibitory barrier to axonal growth. By 28–42 dpi, the C57BL/6J lesion stabilized with the establishment of a dense fibrotic scar core, filled with macrophage profiles and minimal extracellular space, devoid of axons, and surrounded by a distinct glial barrier; this contrasted with the chronic MRL/MpJ lesion and surrounding tissue rim, which supported robust axonal growth in the presence of increased extracellular space, a loose fibronectin and collagen matrix and increased extravascular laminin. The full comparison of the cellular and extracellular features of the lesion site in the two strains is summarized in Table 1. Notably, the complex traits that facilitate axonal growth after SCI in the MRL/MpJ mouse are observed in the context of a reduced local inflammatory response across all time points. This is consistent with the known evolutionary balance between the increasing complexity of the neuroimmune system and failed regeneration due to scar formation (Popovich and Longbrake, 2008). However, the continued remodeling in the regenerative strain appeared to compromise the ability of the CNS to establish and maintain the integrity of the surrounding tissues, and may help explain, in part, why functional recovery is impaired in MRL/MpJ mice despite increased axonal growth at the site of injury.

The increased axon density in the MRL/MpJ lesion, with axons filling 10–15% of the entire lesion volume, is greater than we have seen previously in the context of the mouse contusion injury (Ma et al., 2004; Kigerl et al., 2006). The contusion injury does not completely sever all axons traversing the site of impact, but our time course analyses support the interpretation that the vast majority of these NF-stained profiles represent new axonal processes, as very few were present at 7 or 14 dpi. In addition, the orientation of most of the profiles was not parallel with the longitudinal axis of the cord as would be predicted if spared ascending or descending fiber tracts were displaced over time (Steward et al., 2003). Using immunohistochemical staining, we found that many of the axons contained CGRP, especially those near the dorsal half of the lesion site, but none stained with anti-serotonin antibodies. Based on the preponderance of NF+ containing axons in the lesion center and the recent tract tracing work of Inman and Steward (2003) in a mouse crush injury model, there is a strong possibility that a large proportion of the non-CGRP/non-5HT axons within the lesion arise from primary sensory afferents.

Axon growth requires both a sufficient stimulus and a positive balance of permissive and inhibitory factors to support process extension, adhesion and guidance (McKeon et al., 1995; Condic and Lemons, 2002; Snow et al., 2002; Benowitz and Yin, 2007). The increased axon growth in the MRL/MpJ SCI site is consistent with increased permissive characteristics of the lesion site over time, including an enhanced expression of laminin, reduced inhibitory CSPG-GAGs, and a shift from a dense fibronectin rich core to a more diffuse fibronectin matrix. However, the marked axonal growth within the spinal contusion lesion site that we observed appears to contrast with the results of Hampton et al. (2004) who did not observe regeneration of fibers across an injury site caused by a stab wound to the cortex or a knife-cut of the nigrastriatal pathway in MRL/MpJ mice. There are important distinctions between these studies. Notably, Hampton et al. examined axon growth only through 14 dpi, while we found that the increase in axon density in the spinal cord was not evident until 28–42 dpi. Thus, it is likely that a longer survival time is required to allow the local environmental and extracellular matrix remodeling needed to support regeneration after CNS injury in these mice. Other differences between the injury models suggest that additional underlying cellular mechanisms also contribute to robust axon growth into the lesion site in the spinal cord. For example, the recruitment of circulating inflammatory cells and the extent of damage to the blood–brain barrier are more extensive after a knife cut wound to the spinal cord than the brain, leading to a very different interplay between cellular and extracellular components of the two injury models. Differences in the glial response between a knife cut and contusion injury are also well known (Schnell et al., 1999). Finally, Schwann cell invasion is a more pronounced component of the glial response to injury in the spinal cord than the brain, and peripheral axons are highly responsive to growth alongside invading Schwann cells. We observed extensive Schwann cell invasion in both the C57Bl/6J and the MRL/MpJ lesion site, especially at chronic time points, but quantitative differences were not clearly established. Additional studies are under way to determine the relationship between these cells and the axons within the lesion. Together, the complementary observations of this study and Hampton et al. (2004) further the current belief that the development of an enhanced regenerative capacity is not exclusively dictated by genetic influences, but is also highly dependent on local cellular interactions that exhibit extensive regional and temporal heterogeneity (Popovich and Longbrake, 2008).

Despite the increased axon growth into the injury site, functional recovery was not improved in the MRL/MpJ mouse compared with the C57BL/6J strain. This dichotomy is not uncommon in SCI research, because many interventions that promote measurable axon growth do not result in relevant functional connections (Lu and Tuzcynski, 2008). The BMS functional assessment tool documents the recovery of normal hind limb use during open-field locomotion after a mid-thoracic injury, and it is historically correlated with the extent of damage to ascending and descending white matter tracts after contusion injury (Basso et al., 2006). However, there is no clear outcome measure that is known to correlate directly with new axon growth at the lesion site in a spinal contusion model. Thus, it is feasible that functional connections were not achieved because the time course of study was not sufficient or there were insufficient guidance cues to direct axons to appropriate targets. Notably, in the axolotl—the only adult tetrapod with functional regeneration of the spinal cord—the first identifiable swimming movements after complete cord transection are not seen until 4–8 weeks after injury. Likewise, reorganization of the urodele spinal cord continues for at least 23 months after a lesion (Clarke et al., 1988; Chernoff et al., 2003). Furthermore, if many of the observed axons were of peripheral sensory origin, even successful functional connections may not be evident using the BMS outcome score.

Perhaps more intriguing than the lack of improved function in these mice, however, was the finding that the MRL/MpJ recovery profile was significantly worse than that of the C57BL/6J mice, where prolonged inflammation and both glial and connective tissue scarring were prevalent and axon growth was undetectable. This surprising result is unlikely to be due to

overall strain differences in locomotor ability since the uninjured MRL/MpJ mice demonstrated all of the normal characteristics of locomotion prior to injury and proceeded in their recovery according to the validated sequence observed in many other mouse strains (Basso et al., 2006). A key difference in their performance after injury was the inability to step frequently. The heavier weight of the MRL/MpJ mice might contribute to this; indeed, we have seen prolonged failure of weight supported stepping in male MRL/MpJ mice resulting from dragging of the heavier hindquarters (unpublished observations). In this study, however, female mice were used, and the predominant ability to show supported stepping during testing did not correlate with body weight within the strain. The most likely explanation for the impaired functional recovery is supported by the histological observation of continued deterioration of the cellular organization at the lesion site, including the enhanced contracture of the spinal cord and the loss of tissue integrity in the peripheral white matter rim. Notably, the functional deficits were significant by 14 dpi, which preceded the time course of axonal growth. This suggests that earlier events initiate a unique degenerative process that limits the capacity for functional recovery, while the growth of axons seen later after injury does not lead to new functional connections.

Consistent with the current observations, we have shown previously that both acute and chronic inflammation plays an important role in the orchestration of cellular responses and axon growth after SCI (Popovich et al., 1999; Ma et al., 2004; Jones et al., 2005; Kigerl et al., 2007). Prevention of the early influx of peripheral macrophages after SCI in rats leads to increased deposition of a growth permissive matrix, greater axonal growth into the lesion site and improved functional recovery after spinal contusion injury in rats (Popovich et al., 1999). Likewise, in the 129X1/SvJ mouse strain, a blunted inflammatory response is seen in concert with increased growth of peripheral and centrally derived axons and astrocyte invasion into the lesion site (Ma et al., 2004). In the MRL/MpJ mice, astrocytes did not accompany axons into the lesion site despite the reduced inflammatory cell presence. Other laboratories have shown that in some circumstances, macrophages can enhance axonal regeneration. Transplantation of peripheral nerve activated macrophages adjacent to a spinal transection injury in rats (Lazarov-Spiegler et al., 1996), or stimulation of neurons by macrophage factors released close to the neuronal cell body can facilitate axon growth (Steinmetz et al., 2005; Yin et al., 2006), yet exposure of macrophages to a degenerating optic nerve prior to implantation prevents these growth promoting characteristics (Lazarov-Spiegler et al., 1996). In the MRL/MpJ mice, the reduced inflammatory response was associated with reduced scar formation and increased axon growth. In light of the toxicity of the products of macrophage activation, it is unlikely that the blunted inflammatory response was directly associated with chronic degeneration, but downstream effects of inflammatory cytokine release may indirectly influence the neuroprotective properties of surrounding glial cells.

We observed subtle differences in astrocyte morphology and reduced expression of CSPG-GAGs in the peripheral rim of the MRL/MpJ specimens, suggesting that impaired gliosis may contribute to prolonged degeneration. A robust astrocyte response is essential for restricting inflammation and restoring tissue integrity after SCI. If proliferating astrocytes are depleted from the surrounding scar tissue, inflammatory cells invade the surrounding tissue and continued degeneration ensues (Faulkner et al., 2004). The accumulation of astrocytes at the edge of the SCI site is dependent upon phosphorylation of signal transducer and activator of transcription 3 (STAT3), which is downstream of cytokine signaling. If STAT3 is depleted in nestin-positive cells (Okada et al., 2006) or GFAP-positive astrocytes (Herrmann et al., 2008) after SCI, then astrocyte activation and migration are impaired and stabilization of the wound is altered, leading to continued degeneration and impaired functional recovery. However, unlike these models of impaired astrocyte function, we did not see expansion of inflammatory cells into the peripheral white matter rim. However, it is quite possible that the

astrocyte response in the MRL/MpJ mice was not sufficient to protect the surrounding tissues from other mediators of tissue damage.

The chemical mediators of the degenerative process in MRL/MpJ spinal cord are not known. One strong group of candidates mediating the pathology of the chronic SCI site is the matrix metalloproteases (MMPs), which have been shown to be increased in this strain. MMPs are zinc-dependent proteases that cleave extracellular matrix molecules to facilitate cell migration. The MRL/MpJ mouse has a heightened and prolonged local expression of MMPs, including both MMP-2 and MMP-9, following ear punch or after injury to the cortex or retina in the CNS (Gourevitch et al., 2003; Hampton et al., 2004; Tucker et al., 2008). MMPs are important mediators of tissue regeneration in urodeles (Chernoff et al., 2000; Monaghan et al., 2007), yet their functions after injury in the mammalian CNS are complex. MMP-9 is upregulated at 1–2 days after SCI, during the period of neutrophil recruitment and tissue degradation (Noble et al., 2002; Goussev et al., 2003; Fleming et al., 2006). Depletion of MMP-9 at this acute time point is neuroprotective, supporting the hypothesis that MMP-9 activity contributes to early secondary injury (Noble et al., 2002). In contrast, MMP-2 expression peaks between 5 and 7 dpi and remains high as long as 3 weeks postinjury. MMP-2 is expressed by macrophages, endothelial cells and astrocytes, and is believed to contribute to revascularization and axonal sprouting after injury. A heightened expression of MMPs in the MRL/MpJ retina corresponds to reduced CSPG staining and development of a permissive environment for photoreceptor cell migration (Tucker et al., 2008), while prolonged MMP-2 and MMP-9 expression after the cortical stab wound described above is associated with increased and prolonged blood–brain barrier disruption (Hampton et al., 2004). In the spinal cord contusion model studied here, the possibility of unchecked expression of both MMP-2 and MMP-9 could underlie the both continued degradation of the tissue extracellular matrix extending into the spared tissue regions and the enhanced growth of axons into the lesion site.

Over the course of these experiments, we have reviewed a few of the characteristic features seen in the MRL/MpJ mouse following SCI that are comparable to the successful regenerative wound healing responses of invertebrates and lower vertebrates, including a diminutive inflammatory response and altered composition of the lesion scar. Notably, we did not observe evidence of true spinal cord regeneration as a reflection of a proliferative response or blastema formation as described previously in the ear punch in MRL/MpJ mice or the regenerating tissues of urodeles and invertebrates (Clark et al., 1998; Reddien and Sanchez Alvarado, 2004; Slack et al., 2004). Recently, it has been demonstrated that there is increased proliferation and migration of multipotent neuroblasts within the subventricular zone along the wall of the lateral ventricle of the uninjured adult MRL/MpJ mouse (Baker et al., 2006) suggesting that the MRL/MpJ mouse may have a greater potential to generate multipotent cells in response to injury. We did, however, note the presence of small clusters of cells within the MRL/MpJ lesion with darkened cytoplasm, reminiscent of immature or rapidly dividing progenitors. Further studies in the injured MRL/MpJ spinal cord are warranted to determine if an increased regenerative response in these mice can be stimulated by increasing production or differentiation of endogenous stem or progenitor cells. By identifying and modulating the signals that dictate regenerative and potential degenerative events in this strain, we will be better able to direct strategies to promote repair in the complex environment of SCI in other strains and species, including man.

CONCLUSIONS

Comparison of the pathological evolution of SCI in C57BL/6J and MRL/MpJ mice revealed genetic variation in the cellular response to an identical mechanical injury. The results provide insight into the dynamics of intraspinal inflammation, axonal growth and tissue repair in the CNS. At the most chronic time points, the MRL/MpJ mice develop a uniquely permissive

environment for axonal regeneration. However, an untoward consequence of the complex traits leading to continued remodeling of the extracellular environment is the loss of the ability to restore tissue integrity after insult, which has likely evolved to support cellular homeostasis necessary for optimal function in the mammalian CNS. In the future, the MRL/MpJ mouse strain will serve as a unique tool and model system for evaluating the consequences of manipulating the temporal, cellular and molecular responses to SCI. Findings from genetic models such as this can be exploited to posit new strategies that can take advantage of endogenous repair capacity of the mammalian CNS to promote functional recovery.

Acknowledgements

Pat Walters, Zhen Guan, Qin Feng Yin and Kathy Wolken provided technical support. The authors would like to thank D. McTigue, R. White, E. Hoschouer, K. Kigerl and E. Longbrake for discussion and review. Support: NIH NS043246 (L.B.J.), NS037241 (B.T.S.), NS037846 and NS047175 (P.G.P.) NS045758 (Core facility), DE13749 (SKK; PI R. Glaser).

Abbreviations

ANOVA
: analysis of variance

BBB
: Basso Beattie Bresnahan locomotor rating scale

BMS
: Basso mouse scale for locomotor recovery in mice

CSPG
: chondroitin sulfate proteoglycan

dcc
: darkly stained cytoplasm

dpi
: days post-injury

Fb
: fibroblast

GAG
: glycosaminoglycan

GFAP
: glial fibrillary acidic protein

LFB
: Luxol Fast Blue

MC
: macrophage cluster

MMP
: matrix metalloprotease

NF
: neurofilament

PA

proportional area=stained area/reference area

PBS
phosphate-buffered saline

SCI
spinal cord injury

STAT3
signal transducer and activator of transcription 3

SWM
spared white matter

TCSA
total cross-sectional area

References

Baker KL, Daniels SB, Lennington JB, Lardaro T, Czap A, Notti RQ, Cooper O, Isacson O, Frasca S Jr, Conover JC. Neuroblast protuberances in the subventricular zone of the regenerative MRL/MpJ mouse. J Comp Neurol 2006;498:747–761. [PubMed: 16927265]

Basso DM, Beattie MS, Bresnahan JC. A sensitive and reliable locomotor rating scale for open field testing in rats. J Neurotrauma 1995;12:1–21. [PubMed: 7783230]

Basso DM, Beattie MS, Bresnahan JC. Graded histological and locomotor outcomes after spinal cord contusion using the NYU weight-drop device versus transection. Exp Neurol 1996;139:244–256. [PubMed: 8654527]

Basso DM, Fisher LC, Anderson AJ, Jakeman LB, McTigue DM, Popovich PG. Basso mouse scale for locomotion detects differences in recovery after spinal cord injury in five common mouse strains. J Neurotrauma 2006;23:635–659. [PubMed: 16689667]

Beare AH, Metcalfe AD, Ferguson MW. Location of injury influences the mechanisms of both regeneration and repair within the MRL/MpJ mouse. J Anat 2006;209(4):547–559. [PubMed: 17005026]

Beattie MS, Bresnahan JC, Lopate G. Metamorphosis alters the response to spinal cord transection in Xenopus laevis frogs. J Neurobiol 1990;21:1108–1122. [PubMed: 2258724]

Behrmann DL, Bresnahan JC, Beattie MS, Shah BR. Spinal cord injury produced by consistent mechanical displacement of the cord in rats: behavioral and histologic analysis. J Neurotrauma 1992;9:197–217. [PubMed: 1474608]

Benowitz LI, Yin Y. Combinatorial treatments for promoting axon regeneration in the CNS: strategies for overcoming inhibitory signals and activating neurons' intrinsic growth state. Dev Neurobiol 2007;67:1148–1165. [PubMed: 17514713]

Bresnahan JC, Beattie MS, Todd FD 3, Noyes DH. A behavioral and anatomical analysis of spinal cord injury produced by a feedback-controlled impaction device. Exp Neurol 1987;95:548–570. [PubMed: 3817079]

Chernoff EA, O'Hara CM, Bauerle D, Bowling M. Matrix metal-loproteinase production in regenerating axolotl spinal cord. Wound Repair Regen 2000;8:282–291. [PubMed: 11013020]

Chernoff EA, Sato K, Corn A, Karcavich RE. Spinal cord regeneration: intrinsic properties and emerging mechanisms. Semin Cell Dev Biol 2002;13:361–368. [PubMed: 12324218]

Chernoff EA, Stocum DL, Nye HL, Cameron JA. Urodele spinal cord regeneration and related processes. Dev Dyn 2003;226:295–307. [PubMed: 12557207]

Church JC, Warren DJ. Wound healing in the web membrane of the fruit bat. Br J Surg 1968;55:26–31. [PubMed: 5635416]

Clark LD, Clark RK, Heber-Katz E. A new murine model for mammalian wound repair and regeneration. Clin Immunol Immu-nopathol 1998;88:35–45.

Clarke JD, Alexander R, Holder N. Regeneration of descending axons in the spinal cord of the axolotl. Neurosci Lett 1988;89:1–6. [PubMed: 3399135]

Colwell AS, Krummel TM, Kong W, Longaker MT, Lorenz HP. Skin wounds in the MRL/MPJ mouse heal with scar. Wound Repair Regen 2006;14(1):81–90. [PubMed: 16476076]

Condic ML, Lemons ML. Extracellular matrix in spinal cord regeneration: getting beyond attraction and inhibition. Neuroreport 2002;13:A37–A48. [PubMed: 11930141]

Davies SJ, Fitch MT, Memberg SP, Hall AK, Raisman G, Silver J. Regeneration of adult axons in white matter tracts of the central nervous system. Nature 1997;390:680–683. [PubMed: 9414159]

Davies SJ, Goucher DR, Doller C, Silver J. Robust regeneration of adult sensory axons in degenerating white matter of the adult rat spinal cord. J Neurosci 1999;19:5810–5822. [PubMed: 10407022]

Faulkner JR, Herrmann JE, Woo MJ, Tansey KE, Doan NB, Sofroniew MV. Reactive astrocytes protect tissue and preserve function after spinal cord injury. J Neurosci 2004;24(9):2143–2155. [PubMed: 14999065]

Ferretti P, Zhang F, O'Neill P. Changes in spinal cord regenerative ability through phylogenesis and development: lessons to be learnt. Dev Dyn 2003;226:245–256. [PubMed: 12557203]

Fitch MT, Doller C, Combs CK, Landreth GE, Silver J. Cellular and molecular mechanisms of glial scarring and progressive cavitation: in vivo and in vitro analysis of inflammation-induced secondary injury after CNS trauma. J Neurosci 1999;19:8182–8198. [PubMed: 10493720]

Fitch MT, Silver J. CNS injury, glial scars, and inflammation: Inhibitory extracellular matrices and regeneration failure. Exp Neu-rol 2008;209:294–301.

Fleming JC, Norenberg MD, Ramsay DA, Dekaban GA, Marcillo AE, Saenz AD, Pasquale-Styles M, Dietrich WD, Weaver LC. The cellular inflammatory response in human spinal cords after injury. Brain 2006;129:3249–3269. [PubMed: 17071951]

Fry EJ, Stolp HB, Lane MA, Dziegielewska KM, Saunders NR. Regeneration of supraspinal axons after complete transection of the thoracic spinal cord in neonatal opossums (Monodelphis do-mestica). J Comp Neurol 2003;466:422–444. [PubMed: 14556298]

Goss RJ, Grimes LN. Epidermal downgrowths in regenerating rabbit ear holes. J Morphol 1975;146:533–542. [PubMed: 1171254]

Gourevitch D, Clark L, Chen P, Seitz A, Samulewicz SJ, Heber-Katz E. Matrix metalloproteinase activity correlates with blastema formation in the regenerating MRL mouse ear hole model. Dev Dyn 2003;226:377–387. [PubMed: 12557216]

Goussev S, Hsu JY, Lin Y, Tjoa T, Maida N, Werb Z, Noble-Haeusslein LJ. Differential temporal expression of matrix metalloprotein-ases after spinal cord injury: relationship to revascularization and wound healing. J Neurosurg 2003;99:188–197. [PubMed: 12956462]

Hampton DW, Seitz A, Chen P, Heber-Katz E, Fawcett JW. Altered CNS response to injury in the MRL/MpJ mouse. Neuro-science 2004;127:821–832.

Herrmann JE, Imura T, Song B, Qi J, Ao Y, Nguyen TK, Korsak RA, Takeda K, Akira S, Sofroniew MV. STAT3 is a critical regulator of astrogliosis and scar formation after spinal cord injury. J Neurosci 2008;28(28):7231–7243. [PubMed: 18614693]

Inman DM, Steward O. Ascending sensory, but not other long-tract axons, regenerate into the connective tissue matrix that forms at the site of a spinal cord injury in mice. J Comp Neurol 2003;462:431–449. [PubMed: 12811811]

Jakeman LB, Guan Z, Wei P, Ponnappan R, Dzwonczyk R, Popovich PG, Stokes BT. Traumatic spinal cord injury produced by controlled contusion in mouse. J Neurotrauma 2000;17:299–319. [PubMed: 10776914]

Jones TB, McDaniel EE, Popovich PG. Inflammatory-mediated injury and repair in the traumatically injured spinal cord. Curr Pharm Des 2005;11:1223–1236. [PubMed: 15853679]

Kigerl KA, Lai W, Rivest S, Hart RP, Satoskar AR, Popovich PG. Toll-like receptor (TLR)-2 and TLR-4 regulate inflammation, gliosis, and myelin sparing after spinal cord injury. J Neurochem 2007;102 (1):37–50. [PubMed: 17403033]

Kigerl KA, McGaughy VM, Popovich PG. Comparative analysis of lesion development and intraspinal inflammation in four strains of mice following spinal contusion injury. J Comp Neurol 2006;494:578–594. [PubMed: 16374800]

Kwiecien JM, Avram R. Long-distance axonal regeneration in the filum terminale of adult rats is regulated by ependymal cells. J Neurotrauma 2008;25:196–204. [PubMed: 18352833]

Lane MA, Truettner JS, Brunschwig JP, Gomez A, Bunge MB, Dietrich WD, Dziegielewska KM, Ek CJ, Vandeberg JL, Saunders NR. Age-related differences in the local cellular and molecular responses to injury in developing spinal cord of the opossum, Monodelphis domestica. Eur J Neurosci 2007;25:1725–1742. [PubMed: 17432961]

Lazarov-Spiegler O, Solomon AS, Zeev-Brann AB, Hirschberg DL, Lavie V, Schwartz M. Transplantation of activated macrophages overcomes central nervous system regrowth failure. FASEB J 1996;10:1296–1302. [PubMed: 8836043]

Leferovich JM, Bedelbaeva K, Samulewicz S, Zhang XM, Zwas D, Lankford EB, Heber-Katz E. Heart regeneration in adult MRL mice. Proc Natl Acad Sci U S A 2001;98:9830–9835. [PubMed: 11493713]

Li X, Gu W, Masinde G, Hamilton-Ulland M, Xu S, Mohan S, Baylink DJ. Genetic control of the rate of wound healing in mice. Heredity 2001a;86:668–674. [PubMed: 11595047]

Li X, Mohan S, Gu W, Baylink DJ. Analysis of gene expression in the wound repair/regeneration process. Mamm Genome 2001b;12:52–59. [PubMed: 11178744]

Lu P, Tuzcynski MH. Growth factors and combinatorial therapies for CNS regeneration. Exp Neurol 2008;209(2):313–320. [PubMed: 17927983]

Ma M, Basso DM, Walters P, Stokes BT, Jakeman LB. Behavioral and histological outcome following graded contusion injury in C57Bl/6 mice. Exp Neurol 2001;169:239–254. [PubMed: 11358439]

Ma M, Wei P, Wei T, Ransohoff RM, Jakeman LB. Enhanced axonal growth into a spinal cord contusion injury site in a strain of mouse (129X1/SvJ) with a diminished inflammatory response. J Comp Neurol 2004;474:469–486. [PubMed: 15174067]

McBrearty BA, Clark LD, Zhang XM, Blankenhorn EP, Heber-Katz E. Genetic analysis of a mammalian wound-healing trait. Proc Natl Acad Sci U S A 1998;95:11792–11797. [PubMed: 9751744]

McKeon RJ, Hoke A, Silver J. Injury-induced proteoglycans inhibit the potential for laminin-mediated axon growth on astrocytic scars. Exp Neurol 1995;136:32–43. [PubMed: 7589332]

Monaghan JR, Walker JA, Page RB, Putta S, Beachy CK, Voss SR. Early gene expression during natural spinal cord regeneration in the salamander Ambystoma mexicanum. J Neurochem 2007;101:27–40. [PubMed: 17241119]

Noble LJ, Donovan F, Igarashi T, Goussev S, Werb Z. Matrix metalloproteinases limit functional recovery after spinal cord injury by modulation of early vascular events. J Neurosci 2002;22:7526–7535. [PubMed: 12196576]

Noble LJ, Wrathall JR. Correlative analyses of lesion development and functional status after graded spinal cord contusive injuries in the rat. Exp Neurol 1989;103:34–40. [PubMed: 2912748]

Okada S, Nakamura M, Katoh H, Miyao T, Shimazaki T, Ishii K, Yamane J, Yoshimura A, Iwamoto Y, Toyama Y, Okano H. Conditional ablation of Stat3 or Socs3 discloses a dual role for reactive astrocytes after spinal cord injury. Nat Med 2006;12(7):829–834. [PubMed: 16783372]

Popovich PG, Guan Z, Wei P, Huitinga I, van Rooijen N, Stokes BT. Depletion of hematogenous macrophages promotes partial hindlimb recovery and neuroanatomical repair after experimental spinal cord injury. Exp Neurol 1999;158:351–365. [PubMed: 10415142]

Popovich PG, Longbrake EE. Can the immune system be harnessed to repair the CNS? Nat Rev Neurosci 2008;9(6):481–493. [PubMed: 18490917]

Popovich PG, Wei P, Stokes BT. The cellular inflammatory response after spinal cord injury in Sprague-Dawley and Lewis rats. J Comp Neurol 1997;377:443–464. [PubMed: 8989657]

Reddien PW, Sanchez Alvarado A. Fundamentals of planarian regeneration. Annu Rev Cell Dev Biol 2004;20:725–757. [PubMed: 15473858]

Scheff SW, Saucier DA, Cain ME. A statistical method for analyzing rating scale data: the BBB locomotor score. J Neuro-trauma 2002;19:1251–1260.

Schnell L, Fearn S, Klassen H, Schwab ME, Perry VH. Acute inflammatory responses to mechanical lesions in the CNS: differences between brain and spinal cord. Eur J Neurosci 1999;11:3648–3658. [PubMed: 10564372]

Slack JM, Beck CW, Gargioli C, Christen B. Cellular and molecular mechanisms of regeneration in Xenopus. Philos Trans R Soc Lond B Biol Sci 2004;359:745–751. [PubMed: 15293801]

Snow DM, Smith JD, Gurwell JA. Binding characteristics of chondroitin sulfate proteoglycans and laminin-1, and correlative neurite outgrowth behaviors in a standard tissue culture choice assay. J Neurobiol 2002;51:285–301. [PubMed: 12150504]

Sroga JM, Jones TB, Kigerl KA, McGaughy VM, Popovich PG. Rats and mice exhibit distinct inflammatory reactions after spinal cord injury. J Comp Neurol 2003;462:223–240. [PubMed: 12794745]

Steinmetz MP, Horn KP, Tom VJ, Miller JH, Busch SA, Nair D, Silver DJ, Silver J. Chronic enhancement of the intrinsic growth capacity of sensory neurons combined with the degradation of inhibitory proteoglycans allows functional regeneration of sensory axons through the dorsal root entry zone in the mammalian spinal cord. J Neurosci 2005;25:8066–8076. [PubMed: 16135764]

Steward O, Zheng B, Tessier-Lavigne M. False resurrections: distinguishing regenerated from spared axons in the injured central nervous system. J Comp Neurol 2003;459:1–8. [PubMed: 12629662]

Tucker B, Klassen H, Yang L, Chen DF, Young MJ. Elevated MMP Expression in the MRL mouse retina creates a permissive environment for retinal regeneration. Invest Ophthalmol Vis Sci 2008;49:1686–1695. [PubMed: 18385092]

Ueno M, Lyons BL, Burzenski LM, Gott B, Shaffer DJ, Roopenian DC, Shultz LD. Accelerated wound healing of alkali-burned corneas in MRL mice is associated with a reduced inflammatory signature. Invest Ophthalmol Vis Sci 2005;46:4097–4106. [PubMed: 16249486]

Wang XM, Terman JR, Martin GF. Evidence for growth of supraspinal axons through the lesion after transection of the thoracic spinal cord in the developing opossum *Didelphis virginiana*. J Comp Neurol 1996;371:104–115. [PubMed: 8835721]

Werner S, Krieg T, Smola H. Keratinocyte-fibroblast interactions in wound healing. J Invest Dermatol 2007;127:998–1008. [PubMed: 17435785]

Yin Y, Henzl MT, Lorber B, Nakazawa T, Thomas TT, Jiang F, Langer R, Benowitz LI. Oncomodulin is a macrophage-derived signal for axon regeneration in retinal ganglion cells. Nat Neurosci 2006;9:843–852. [PubMed: 16699509]

Zhang Z, Fujiki M, Guth L, Steward O. Genetic influences on cellular reactions to spinal cord injury: a wound-healing response present in normal mice is impaired in mice carrying a mutation (WldS) that causes delayed Wallerian degeneration. J Comp Neu-rol 1996;371:485–495.

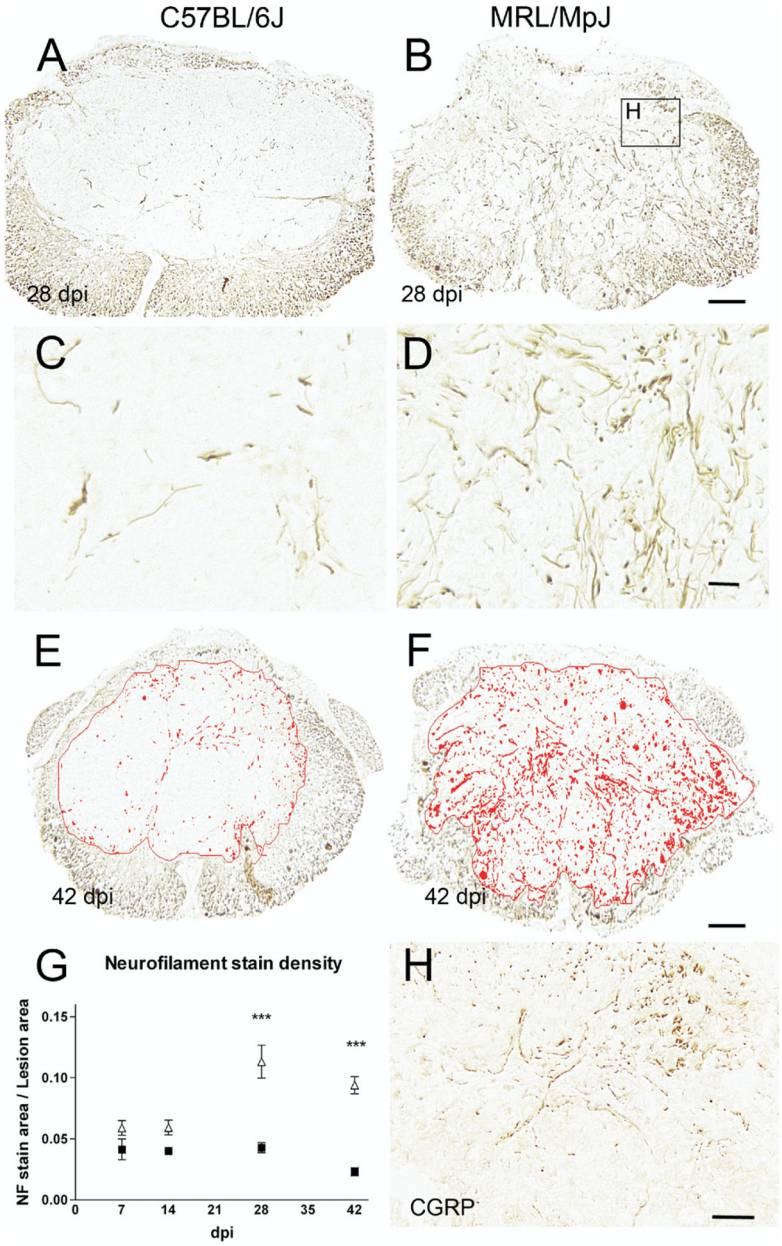

Fig. 1.

NF immunostaining reveals extensive axonal growth within the center of a contusion lesion in MRL/MpJ, but not C57BL/6J mice. Transverse sections through the lesion epicenter from C57BL/6J (A, C, E) and MRL/MpJ (B, D, F) specimens taken at 28 (A–D) and 42 (E, F) dpi, no differences were seen at 7 or 14 dpi. C and D are enlargements from the center of the lesion in specimens from A and B, respectively. (E, F) Axon profiles were quantified by identifying the density threshold for positive staining in the lesion site as indicated by the red binary overlay. Scale bar=100 μm (B, F for A, B and E, F); 20 μm (D for C, E). (G) The PA occupied by axons is greater in MRL/MpJ mice (open triangles) than in C57BL/6J mice (black squares). Two-way ANOVA indicated significant effects of strain (P<0.001; F=77.6, df=1), dpi (P<0.001; F=6.9, df=3) and an interaction effect (P<0.001; F=8.96, df=3) with MRL/MpJ greater at 28 and 42 dpi (P<0.001). (H) CGRP immunoreactivity from a section close to the

NF stained section in B. A subset of the axons in the 28-day MRL/MpJ lesion exhibits CGRP-immunoreactivity (scale bar=10 μm).

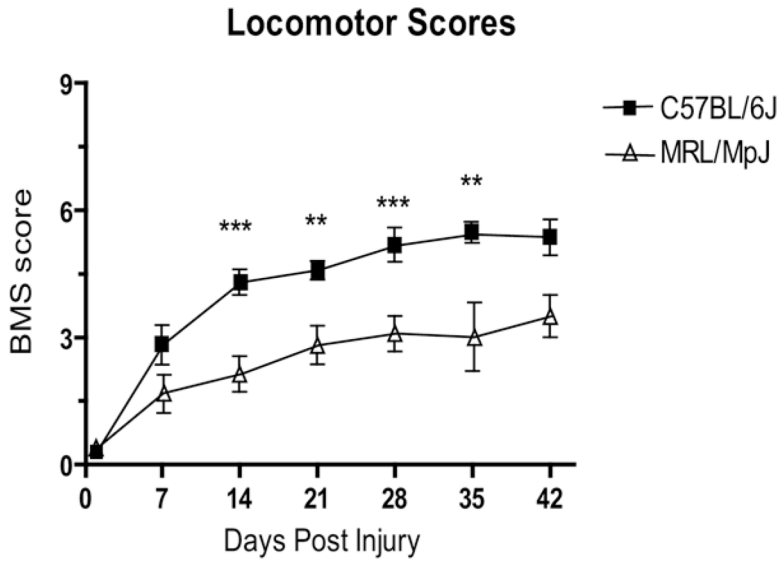

Fig. 2.

Behavioral recovery after SCI is worse in MRL/MpJ mice (open triangles) than C57BL/6J mice (black squares) (two-way ANOVA strain $P<0.001$; dpi $P<0.001$; interaction $P<0.05$; post hoc Bonferroni $P<0.001$ at 14, 28 dpi, $P<0.01$ at 21, 35 dpi).

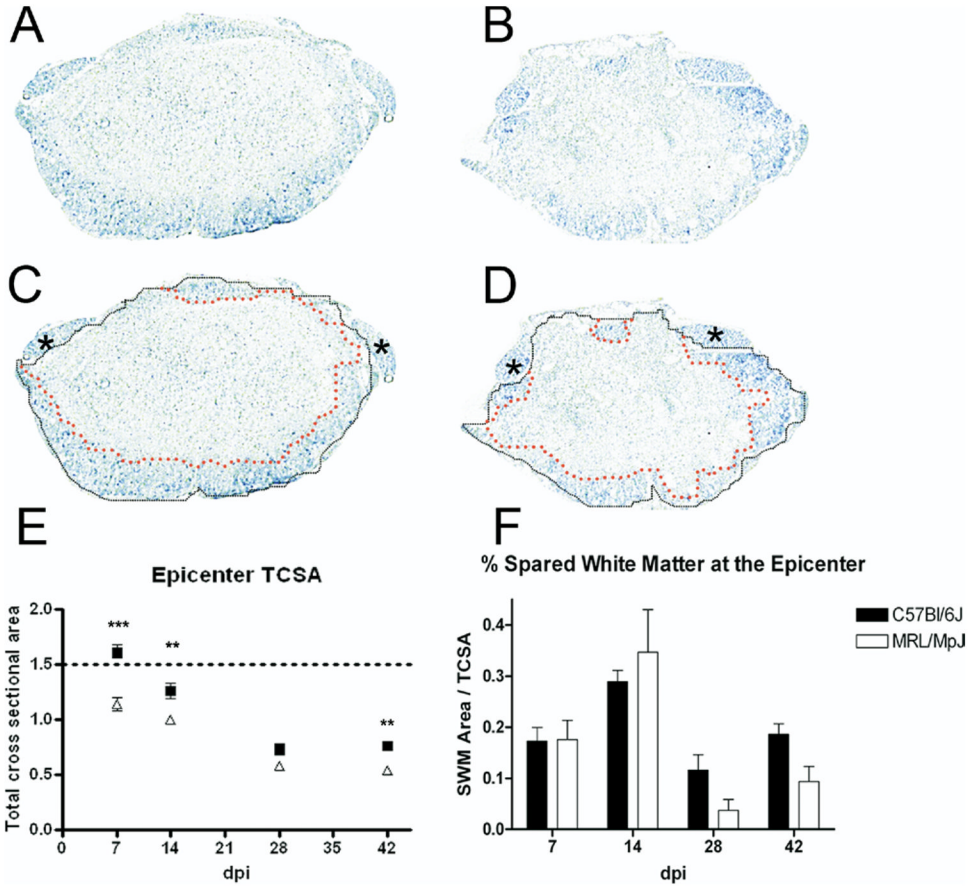

Fig. 3.

LFB-stained sections from the lesion site in C57BL/6J (A, C) and MRL/MpJ (B, D) mice at 42 dpi reveal subtle differences in the evolution of the lesion epicenter using classical white matter sparing measures. (A, B) Sections from both strains show a similar injury pattern including a central region of damage and a rim of peripheral SWM (F). (C, D) The same specimens with outlines to illustrate details of analysis. The TCSA of the section is outlined in black; asterisks identify dorsal roots, which were excluded from analysis. The inner rim of peripheral SWM is outlined in red. Scale bar=200 μm (A–D). (E) TCSA at the epicenter was smaller in MRL/MpJ mice (white triangles) than in C57BL/6J mice (black squares) at 7, 14 and 42 dpi. Dotted line depicts TCSA of uninjured spinal cord. Two-way ANOVA, $P<0.0001$ for strain and dpi; interaction $P<0.01$; Bonferroni post hoc ** $P<0.01$, *** $P<0.001$. (F) SWM at the rim expressed as a percent of cross-sectional area over time. Two-way ANOVA revealed an effect of dpi ($P<0.001$), but no effect of strain ($P>0.05$) or interaction ($P>0.05$). For interpretation of the references to color in this figure legend, the reader is referred to the Web version of this article.

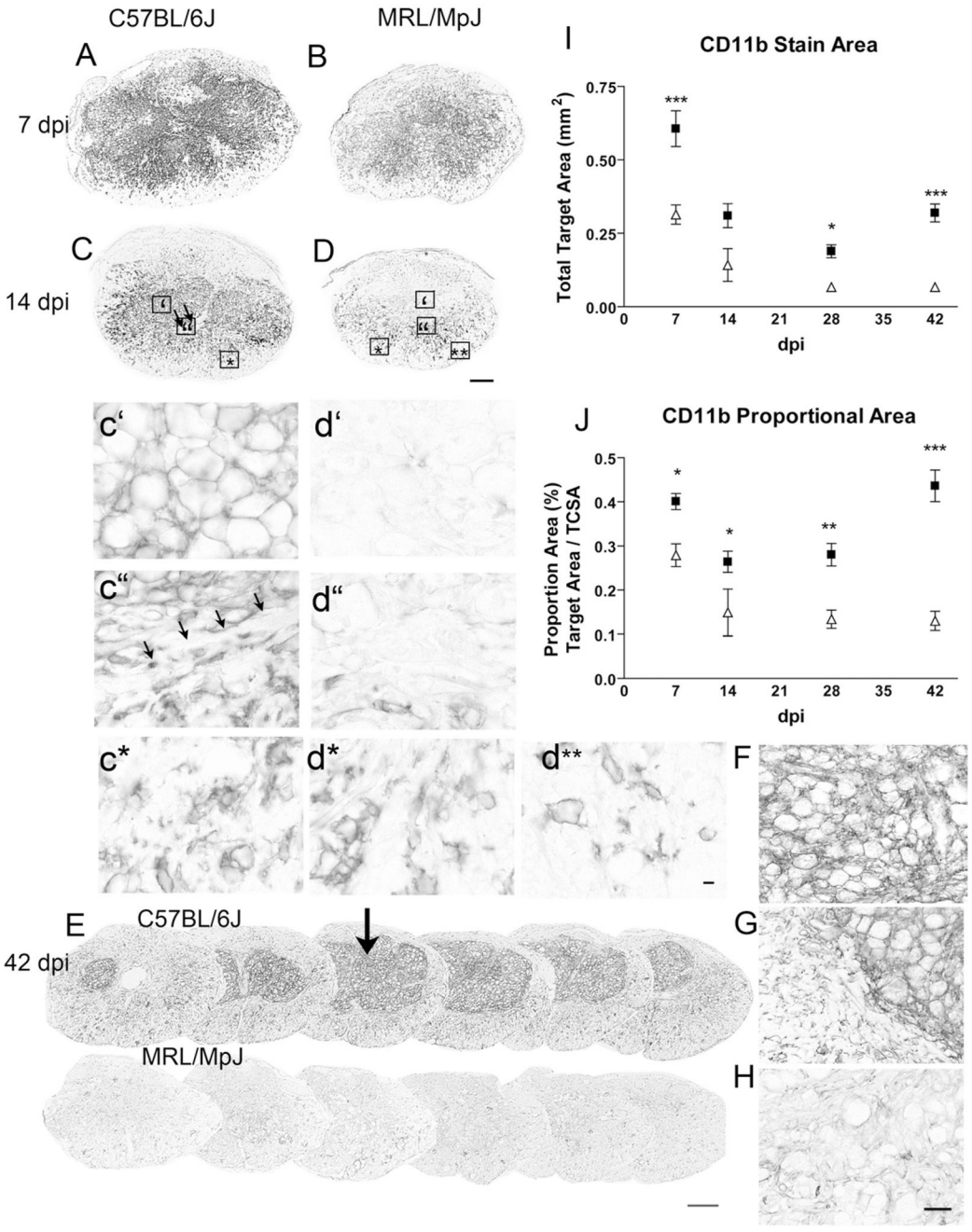

Fig. 4.

CD11b (Mac-1) immunoreactivity was diminished in MRL/MpJ mice at all time points examined. Corresponding sections from the epicenter of C57BL/6J (A, C, E–G) and MRL/MpJ (B, D, E, H) specimens were stained simultaneously. (A) Macrophages are found throughout the lesion center in both strains at 7 dpi. (B) The area and intensity of Mac-1 staining were lower in MRL/MpJ mice; (C) 14 dpi in C57BL/6J mice. Boxes indicate regions enlarged below. The lesion contains a large area of Mac-1 staining, with rounded MCs throughout the center (c′), and a thin rim devoid of Mac-1 staining bordering the clusters (c″ arrows). Below this rim, activated Mac-1 positive cells exhibit heterogeneous morphologies suggesting a microglial origin. (D) Little to no staining was found in the lesion center in the MRL/MpJ mice

at 14 dpi (d″), while elongated Mac-1+ cells line the borders (d″). Both strains have similar microglial distribution and activation in the rim of white matter (c*, d*, d**); (E) 42 dpi. Mac-1-stained sections spaced 300 μm apart through the lesion site in representative animals at 42 dpi illustrating the marked reduction in macrophage staining in MRL/MpJ mice at this chronic time point. The lesion epicenter section is marked by the arrow. (F–H) Enlargements from the sections stained at 42 dpi. (F) Center of a C57BL/6J lesion. (G) Border of the lesion center in C57BL/6J specimen. (H) Center of an MRL/MpJ lesion. (E, I, J) Time course of total (I) and proportional (J) area measures of Mac-1 (CD11b) labeled-macrophage/microglial profiles at the epicenter section in C57BL/6J and MRL/MpJ specimens Two-way ANOVA effect of dpi and strain for both measures ($P<0.0001$), differences between strains at each time point marked with asterisks (* $P<0.05$, ** $P<0.01$, *** $P<0.0001$). Scale bar=200 μm A–E; d**: Scale bar=10 μm c–d**. Scale bar=50 μm F–H.

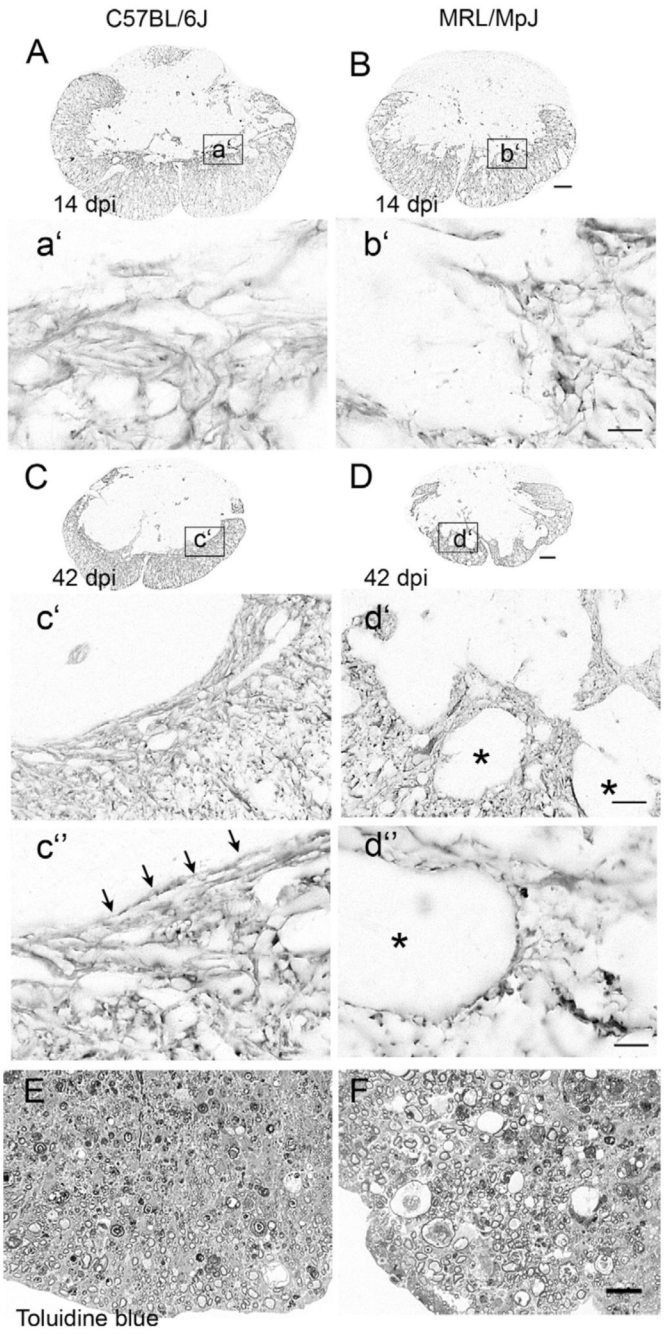

Fig. 5.

The astrocyte border and peripheral rim shows greater heterogeneity of staining and increased extracellular space in MRL/MpJ mice. (A, B) Low power micrographs of GFAP stained epicenters at 14 dpi. Staining patterns are similar in both strains. Enlargements (a′, b′) show the developing glial border containing cells and processes. (C, D) Low power micrographs 42 dpi. Enlargements (c′, d′) reveal differences in composition of the peripheral rim, which is homogeneous in the C57BL/6J mice and forms a clear and straight border at the lesion edge (c′) while the MRL/MpJ astrocyte border is occupied by ovoid cysts (d″, asterisks). High power images of the lesion edge (c″, d″) show the aligned glial processes at the lesion edge in C57BL/6J and punctuate glial processes at the edges of the ovoid cavities in the MRL/MpJ mice. (E,

F) Toluidine Blue–stained 1 μm thick sections from the peripheral rim at the lesion center at the same time point. The C57BL/6J white matter (E) is tightly packed, while the MRL/MpJ white matter (F) is characterized by a disorganized parenchyma with larger, more plentiful vacuoles. Scale bar=50 μm (A–D); 200 μm (c′, d′); 10 μm (a′, b′, c″, d″).

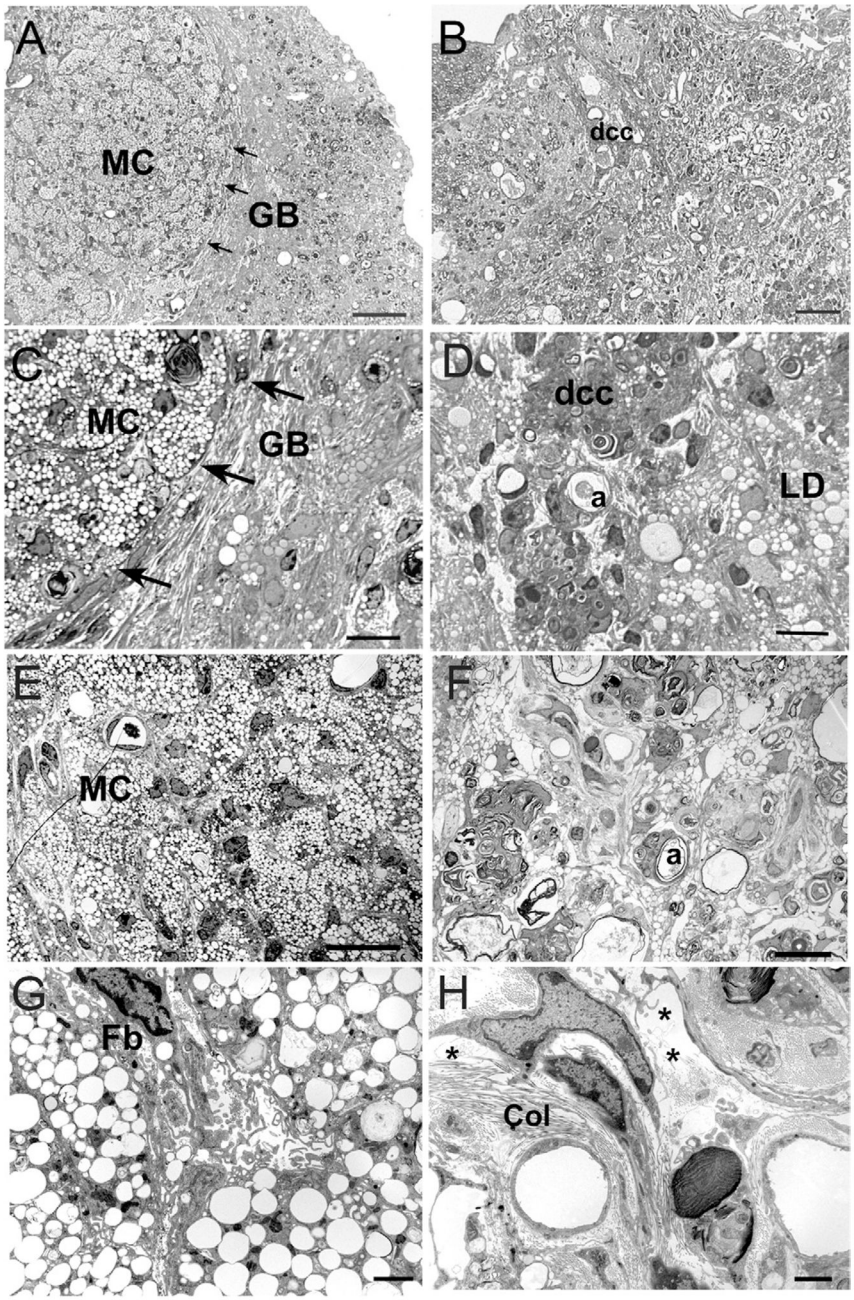

Fig. 6.

Light and electron microscopy through the epicenter reveals a compact composition in C57BL/6J (A, C, E, G) and diffuse cellular organization in MRL/MpJ (B, D, F, H) specimens at 42 dpi. (A–D) Light micrographs from the lateral border of the lesion zones. (A, C) In C57BL/6J mice, packed MC are clearly isolated from a dense glial bundle that surrounds the lesion (GB, arrows). (B, D) The glial border in MRL/MpJ specimens is complex and poorly delineated. MRL/MpJ specimens lack large clusters of macrophages, but contain scattered lipid droplets (LD), degenerating axons (a) and loosely packed tissue elements. Note the presence of clusters of cells with dcc. (E–H) Light (E, F) and electron (G, H) micrographs from the center of the lesion sites. (E, G) C57BL/6J lesions are filled with tightly packed MC and Fb-like cells. (F, H) In MRL/MpJ specimens, degenerating axons (a) are interspersed with lipid droplets (LD)

and lightly stained cell clusters, often found surrounding blood vessels. (H) Higher magnification illustrates the presence of abundant extracellular space (*) and numerous collagen fibers (Cl) throughout the MRL/MpJ lesions. Scale bar=50 μm (A, B); 20 μm (C, D); 10 μm (E, F); 2 μm (G, H).

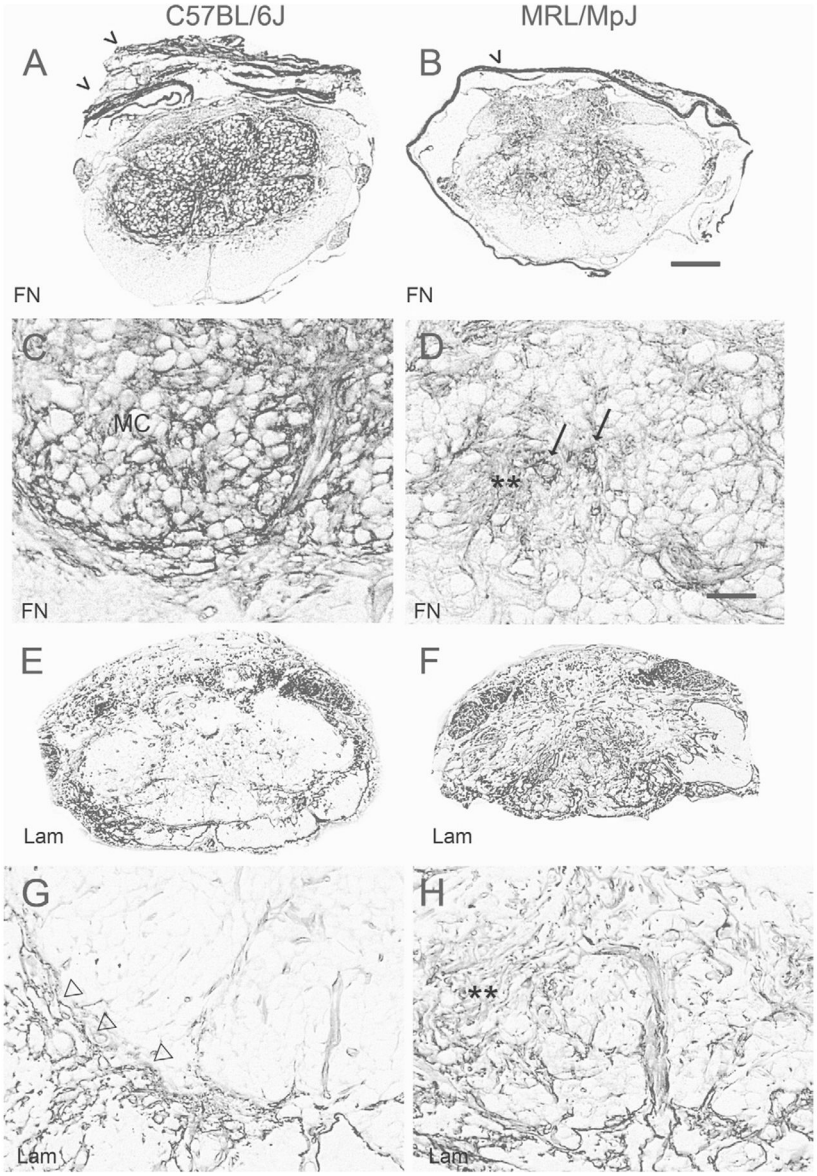

Fig. 7.

The distribution of extracellular matrix molecules at the site of injury at 42 dpi. (A–D) Fibronectin staining is dense throughout the lesion in C57BL/6J mice (A, C), where it fills the center of the lesion, demarcating the lesion border and individual unstained spheres of macrophages. In contrast, staining in the MRL/MpJ specimens at this time (B, D) is more diffuse. Staining is found in patches (**) and associated with cellular profiles (arrows) in this strain. (E–H) Laminin is evident in the lesion border and dorsal roots of both strains at 42 dpi. In C57BL/6J mice (E, G), staining within the lesion is restricted primarily to blood vessels. In contrast, laminin staining is widely distributed throughout the damaged regions of MRL/MpJ mice (F, H), where it is associated with blood vessels and also distributed in patches away from vessels (**). Scale bar=200 μm (A, B, E, F); 50 μm (C, D, G, H).

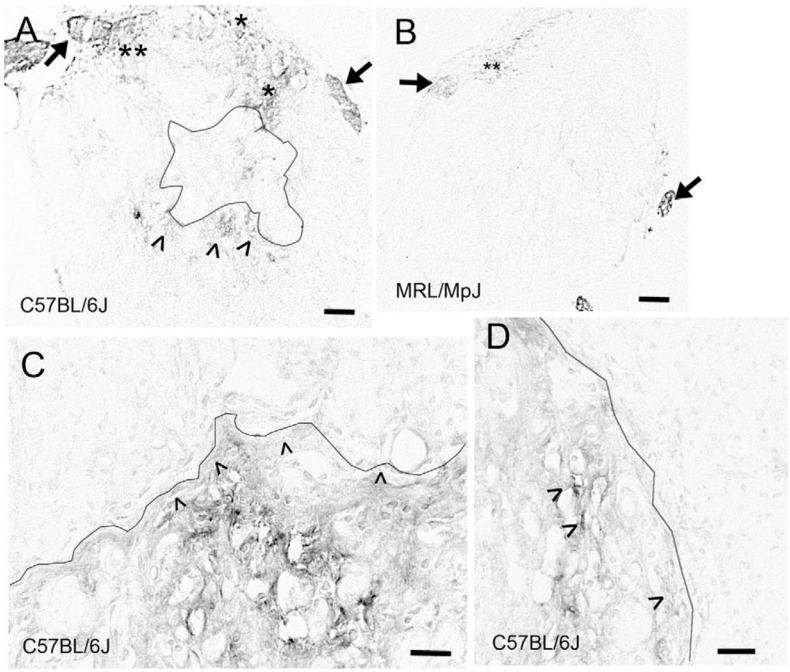

Fig. 8.

Representative images of CS56 staining at 14 dpi in C57BL/6J (A, C, D) and MRL/MpJ (B) specimens. CS56 is upregulated in the dorsal roots (arrows) and at the dorsal root entry zone (asterisks) in both strains. In the C57BL/6J mice, CS56 staining is also associated with cells near to (^) and with the extracellular matrix directly apposed to the lateral and ventral borders of the lesion site (black outline). (C, D) Enlarged photomicrographs from a nearby section of the same specimen as A, showing the extracellular expression of CS56 immunoreactivity along the ventral (C) and lateral (D) border of the lesion center. Staining was very low or below the level of detection at the lesion border in the MRL/MpJ mice. Scale bar=50 μm (A, B); 20μm (C, D).

Table 1

Anatomical changes after SCI in C57BL/6J and MRL/MpJ mice

Features	C57BL/6J	MRL/MpJ
Axonal density in the lesion*	3–5% Of total lesion volume	10–15% Of lesion volume
Epicenter TCSA*	Smaller than uninjured at 28, 42 dpi	Smaller than uninjured at 7, 14, 28 and 42 dpi
Spared white matter PA[ns]	5–20%	5–20%
Macrophage response—area occupied by Mac-1*	30–50% Of lesion area, increasing with time	Initial recruitment, decreasing with time, <10% of lesion area at 28, 42 dpi
Spared rim tissue density	Compact, homogeneous	Vacuous, disorganized
Lesion border definition	Well-defined glial limitans	Irregular border, poorly demarcated
Lesion center cytoarchitecture	Compact, minimal extracellular space	Heterogeneous and loose
Epicenter profiles, 42 dpi	Tightly packed macrophage clusters	Loose structure, absent of macrophages
Lesion matrix composition	Fibronectin predominant	Laminin predominant
CSPG deposition	Prominent at astrocyte borders and dorsal roots at 7–14 dpi	Found in dorsal roots only at 7–14 dpi

Comparison of cellular changes after SCI in C57BL/6J and MRL/MpJ mice. Characteristics of the lesion evolution in the two mouse strains.

* Indicates quantitative analysis of the measured parameters revealed significant differences in outcome ($P<0.05$). ns, no significant difference; PA, area of white matter rim/total cross sectional area at the lesion epicenter.